Aerial Vision Based Guidance and control for Perception-Less Ground Vehicle

M. Ferreira Santos, Pedro Castillo Garcia, Alessandro Corrêa Victorino

▶ **To cite this version:**

M. Ferreira Santos, Pedro Castillo Garcia, Alessandro Corrêa Victorino. Aerial Vision Based Guidance and control for Perception-Less Ground Vehicle. 22nd European Control Conference (ECC 2024), Jun 2024, Stockholm, Sweden. pp.2780-2785, 10.23919/ECC64448.2024.10590923 . hal-04792357

HAL Id: hal-04792357

https://cnrs.hal.science/hal-04792357v1

Submitted on 20 Nov 2024

HAL is a multi-disciplinary open access archive for the deposit and dissemination of scientific research documents, whether they are published or not. The documents may come from teaching and research institutions in France or abroad, or from public or private research centers.

L'archive ouverte pluridisciplinaire **HAL**, est destinée au dépôt et à la diffusion de documents scientifiques de niveau recherche, publiés ou non, émanant des établissements d'enseignement et de recherche français ou étrangers, des laboratoires publics ou privés.

Aerial vision based guidance and control for perception-less ground vehicle

M. Ferreira Santos[1], P. Castillo[1] and A. Corrêa Victorino[1]

***Abstract*— The synergy between unmanned aerial vehicles (UAVs) and unmanned ground vehicles (UGVs) within a heterogeneous system presents diverse avenues for cooperative operation. These collaborations leverage the complementary strengths of both systems, culminating in remarkable improvements in task execution efficiency. In this paper, we explore the concept of a perception-sensor-deprived UGV, and introduce a ground vehicle guidance and control system that exclusively relies on aerial perception to perform path-following tasks. The cooperative architecture is composed of two parts, one for detecting and tracking the ground trajectory using aerial images retrieved from the UAV. And the second for computing the control inputs for ground autonomous navigation. A nonlinear controller for the ground vehicle is designed using sliding mode with fractional components and its stability analysis is proved using the Lyapunov theory. The cooperative architecture was proved in real-time tests showing that experimental results underscore the well efficacy of this system in autonomously guiding a ground vehicle along a predefined path solely based on aerial imagery, opening new horizons for advanced robotics and autonomous systems. To our best of knowledge, this represents the inaugural endeavor in the development of a car-like robot dynamics controller based on non-stationary aerial imagery for path following utilizing a non-learning approach.**

I. INTRODUCTION

In the realm of robotics systems, the synergy between Unmanned Aerial Vehicles (UAVs) and Unmanned Ground Vehicles (UGVs) within heterogeneous systems can manifest in various modes, where the unique capabilities of each component complement one another, yielding enhanced efficiency in task execution. Consequently, numerous researchers have delved into scientific research of such robotic systems. For example, to illustrate in the pursuit of augmenting UGV traversability, authors in [1] employed UAVs to assist ground robots in overcoming challenging terrains, such as cliffs. Similarly, authors in [2] designed a tether-connected UAV-UGV system that combines the merits of both aerial and ground-based robots.

Furthermore, taking inspiration from the cooperative hunting behavior observed in wolves and ravens, a distributed robust controller for aerial-ground vehicle collaboration, aimed at tracking moving targets, was proposed in [3]. This inventive control system exemplifies how UAVs and UGVs can harmonize their operations, emulating natural synergies observed in the animal kingdom to accomplish complex tasks efficiently.

[1]M. Ferreira, A. Correa and P. Castillo are with the Université de technologie de Compiegne, Heudiasyc laboratory UMR CNRS 7253, Compiegne, France. (mferrreir, castillo, acorreav)@hds.utc.fr

Moreover, several research endeavors have centered their attention on the utilization of aerial vehicles as sensing platforms in collaborative efforts. For example, in [4], a quadcopter is deployed to track a ground mobile robot, thereby supplying crucial imagery support for humanitarian demining operations. In [5] a concept of UAV-UGV collaboration tailored to the specific context of agricultural mapping is introduced. Also, in [6] this cooperative paradigm is extended by employing micro aerial vehicles equipped with loosely coupled localization systems alongside UGVs to offer an advantageous third-person perspective for teleoperation tasks as needed. From previous works, it is clear to see that UAV can enhance the robotics system perception. This led to the development of many path planning solutions based on aerial images. In addition, the evident capability of UAVs to augment the perception capabilities of robotics systems has spurred significant advancements in the field. This progress has consequently lead to path planning solutions that rely on aerial imagery as their foundational input, as evidenced by prior research [7], [8], [9], [10].

To address the UGV controller, in [11] authors focused on controlling a UGV to a desired pose based on aerial images. It is accomplished by using a moving airbone camera system from a remote controlled aircraft, and a static reference object for euclidean reconstruction based on geometric model to compute the UGV pose error. Another study presents an approach for ground vehicle motion control based on visual input, utilizing a stationary overhead camera as detailed in [12]. Relying on learning approaches in [13] authors proposed a UGV collision free motion planning algorithm, where an aerial vehicle serves as a sensing for partial observation of the environment without reconstruction.

Aerial vehicles offer distinct advantages over their ground-based counterparts, chiefly attributable to their expansive field of vision and the inherent capacity to mitigate blind spots through the use of onboard cameras. This heightened visual perspective, particularly relevant in the context of critical sectors such as mining and areas with suboptimal adherence on road surfaces, enables the aerial platform to discern intricate details. Furthermore, due to its better mobility capacity, the UAV can be used as assistance in situations where the ground vehicle's perception sensors fail.

In this work, we introduce a novel ground vehicle control system with an aerial perception capability tailored for path-following applications. This approach involves the deployment of an aerial vehicle equipped with a camera, which hovers at a specified altitude above the ground vehicle devoid of perception sensors. The imagery captured by the aerial

camera is subsequently used for guiding the UGV along a reference path on the ground. To out best knowledge, this is the first work dealing with car-like robot dynamics controller based on non-stationary aerial images with a non-learning approach. Similar works uses the visual servoing controller for lane following tasks, however with the camera onboard to the ground vehicle [14], [15].

The paper is organized as follows; in Section II some mathematical concepts used in the control algorithm are done. In Section III the problem statement is illustrated. In section IV our cooperative architecture is presented. In this section, the vision and control modules are given in detail. Section V is used to illustrate and explain main graphs obtained from experimental results. Finally, in section VI some conclusions and perspectives of this work are mentioned.

II. PRELIMINARIES

The fractional-order derivative-integral operator, from time t_0 to time t, is represented as follows [16]:

$$ {}_{t_0}D_t^{\beta} f(t) = \begin{cases} \frac{d^{\beta}}{dt^{\beta}} & \beta > 0 \\ 1 & \beta = 0 \\ {}_{t_0}I_t^{\beta} = \int_{t_0}^{t} (dt)^{-\beta} & \beta < 0 \end{cases} \tag{1} $$

where β is the fractional order and ${}_{t_0}D_t^{\beta}$ is the fractional operator symbol. Also the composition property ${}_{t_0}D_t^{\beta_i}\,{}_{t_0}D_t^{\beta_j} f(t) = {}_{t_0}D_t^{\beta_1+\beta_j} f(t)$ holds true when $0 \leq \beta_i + \beta_j < 1$, with $\beta_i,\ \beta_j \in (0,1]$. The definition of the fractional derivative and fractional integral are given bellow.

Fractional derivative

The Riemann–Liouville definition of fractional derivative ${}_aD_t^{\beta}$ of a function $f(t)$ [17], can be written as

$$ {}_{t_0}D_t^{\beta} f(t) = \frac{1}{\Gamma(1-\beta)} \frac{d}{dt} \int_{t_0}^{t} (t-\tau)^{-\beta} f(\tau) d\tau \tag{2} $$

where $0 < \beta < 1$. An approximation of this formulation is given in the following equation

$$ {}_{t_0}D_t^{\beta} f(t) \simeq \sum_{n=0}^{N} \binom{\beta}{n} \frac{1}{\Gamma(n+1-\beta)} (t-a)^{n-\beta} f^{(n)}(t) \tag{3} $$

$$ \binom{\beta}{n} = \frac{(-1)^{n-1}\beta\Gamma(n-\beta)}{\Gamma(1-\beta)\Gamma(n+1)} $$

where N is the number of derivatives.

Fractional integral

The Riemann–Liouville definition of fractional integral [18] is denoted as

$$ {}_{t_0}I_t^{\beta} f(t) = \frac{1}{\Gamma(\beta)} \int_{t_0}^{t} (t-\tau)^{\beta-1} f(\tau) d\tau \tag{4} $$

where $\beta > 0$. An approximation of this formulation is given in the following

$$ {}_{t_0}I_t^{\beta} f(t) \simeq \frac{1}{\Gamma(\beta)} \sum_{n=0}^{N} \frac{(-1)^n (t-t_0)^{n+\beta}}{(n+\beta)n!} f^{(n)}(t) \tag{5} $$

where N is the number of derivatives

III. PROBLEM STATEMENT

As previously stated, both ground and aerial vehicles exhibit distinct advantages and limitations. Ground Vehicles (GVs) offer superior autonomy but are constrained by limited perception capabilities and mobility restrictions. Conversely, aerial vehicles possess lower autonomy levels but benefit from expansive perceptual coverage and the ability to mitigate blind spots through onboard cameras. The integration of these vehicles within a heterogeneous cooperative system enables the mutual supplementation of their capabilities, ultimately enhancing task execution efficiency.

Our goal in this work, is to propose a solution for autonomous navigation of a ground vehicle without perception, i.e., we consider that the perception sensors of the ground vehicle are not working and the ground vehicle needs to navigate in an unknown road. For solving this problem, we propose to use an aerial vehicle capable to track a road and observe the scene between the ground vehicle and its close environment, see Figure 1. Therefore, the aerial vehicle can estimate the ground vehicle position relative to it-self or to the path and generate desired positions for the ground vehicle.

In the proposed collaborative system, the aerial vehicle is flying at a specified altitude above a ground vehicle devoid of perception sensors. Positioned atop the ground robot an AruCo marker is strategically placed to ensure detection by the aerial vehicle's onboard camera system. For better illustrating the application, we consider a path composed of both left and right lines, and the objective entails guiding the ground vehicle along this path through the application of an aerial visual servoing approach.

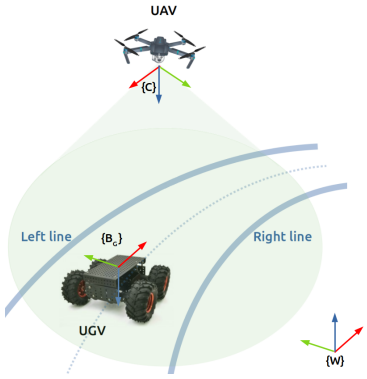

Fig. 1. UAV and UGV navigation

IV. MAIN RESULTS

Our cooperative system, composed by a vision and a control modules with their assigned tasks, is illustrated in Figure 2. In the first module, the desired path and commands for the ground vehicle are computed. These values are estimated using an aerial vision-based algorithm for estimating the ground vehicle pose and the road. The second module uses the information provided by the vision module for calculating the control inputs for trajectory tracking and autonomous

ground navigation. Notice that the aerial vehicle moves as the ground vehicle tracks the trajectory.

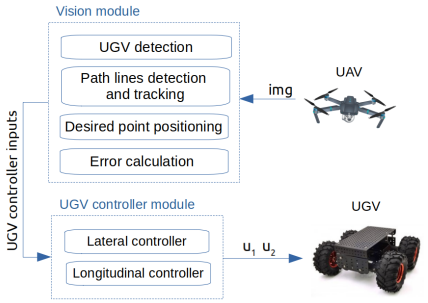

Fig. 2. The cooperative system flowchart.

A. Vision module

This module includes the following image processing tasks: UGV detection, path lines detection and tracking, desired point positioning ($\xi^i_{G_d}$), and UGV error measurement in image frame (i) (where the former is achieved by detecting an ArUco marker located on the top of the ground vehicle).

The goal in this paper is not to introduce a control algorithm for the aerial vehicle, we use a controller from our previous work that assures trajectory tracking for the aerial vehicle, see [19]. The desired trajectory for the aerial vehicle represented in the world frame (W), $\xi^W_{A_d}$, is composed by predefined waypoints with an initial position defined as $\xi^W_{A_{d_0}} = [x^W_{A_{d_0}}, y^W_{A_{d_0}}, z^W_{A_d}]^T$, where $z^W_{A_d}$ is the desired altitude (chosen to be constant during the mision) for the aerial drone. For a quick development of the experiment $\xi^W_{A_{d_0}}$ is chosen to be close to the initial position of the ground vehicle, $\xi^W_{G_{d_0}}$ for being detected by the aerial vehicle as can be seen in Figure 1. Once the aerial vehicle reaches the desired altitude, it begins the aerial trajectory tracking, $\xi^W_{A_d}$.

During the aerial trajectory tracking, the aerial vision algorithm detects the ground vehicle and the road estimating the desired trajectory for the ground vehicle and the error of the trajectory tracking. This task is achieved on 3 main steps. First path lines image points are extracted from images through color based segmentation, see Figure 3. Then the pixel points related to the lines are used for squared line fitting; for both left and right line. Only points inside the regions of interest (ROIs) are considered here, one for the right line and the other for the left line, where their positions and sizes are updated every iteration based on the last detection. In the first iteration there is no previous information about the ROIs, so Hierarquical Agglomerative Clustering algorithm [20] is used to find the two corresponding points of the two lines. The last step comprises the tracking aspect, where an Extended Kalman Filter is used for predicting and updating the lines polygon coefficients, see Figure 4.

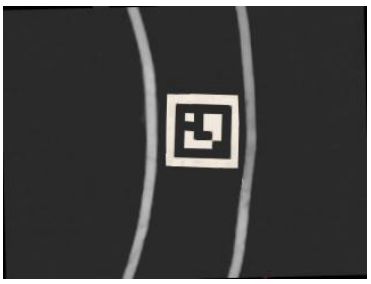

Fig. 3. Aerial image: path lines and the AruCo marker indicating the ground vehicle position.

From the vision algorithm, it is possible to estimate (using the ArUco marker) the position of the ground vehicle in the image plane (ξ^i_G) and its orientation (ψ^i_G) with respect to the x image axis (X^i). Similarly, from the ROIs of the lines, the nearest point (in the center lines) to the UGV is also computed ($\xi^i_{G_{np}}$). To guide the ground vehicle in the path, the desired point ($\xi^i_{G_d}$) for the UGV is positioned at distance L_{la} to the point $\xi^i_{G_{np}}$. The desired orientation $\psi^i_{G_d}$ corresponds to the tangent angle at point $\xi^i_{G_d}$, see Figure 4. Finally, the errors $\bar{e}^i_G = [e^i_{G_x}, e^i_{G_y}, e^i_{G_\psi}]^T$ are calculated on image frame by computing the difference between the desired pose and UGV current pose. These calculated errors are then used as input in the UGV control module.

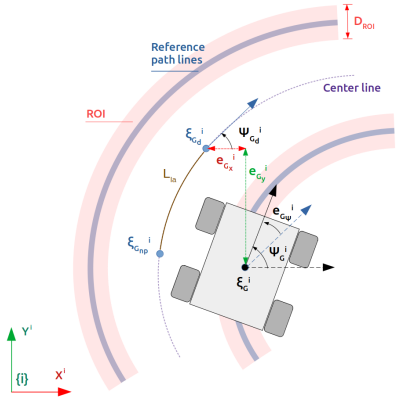

Fig. 4. Information extracted from aerial image. From figure, $D_{ROI} = \lambda_{ROI}/z^W_A$, with λ_{ROI} is a positive constant parameter value and z^W_A is the UAV altitude.

B. Control module

1) UGV dynamic model: From Figure 5, the mathematical equations for the ground vehicle can be defined as,

$$\begin{aligned} m(\ddot{x}^{B_G}_G - \dot{y}^{B_G}_G \dot{\psi}^{B_G}_G) &= F_{x_r} + F_{x_f}\cos(\delta) - F_{y_f}\sin(\delta) \\ m(\ddot{y}^{B_G}_G - \dot{x}^{B_G}_G \dot{\psi}^{B_G}_G) &= F_{y_r} + F_{x_f}\sin(\delta) - F_{y_f}\cos(\delta) \\ I_z \ddot{\psi}^{B_G}_G &= l_f(F_{x_f}\sin(\delta) + F_{y_f}\cos(\delta)) - l_r F_{y_r} \end{aligned} \quad (6)$$

where I_z is vehicle yaw inertia, m the vehicle mass, $\dot{x}^{B_G}_G$ and $\dot{y}^{B_G}_G$ are the vehicle velocities, $\ddot{x}^{B_G}_G$ and $\ddot{y}^{B_G}_G$ denotes the vehicle accelerations, F_{y_f} and F_{y_r} describe the lateral forces in the ground vehicle, F_{x_f} and F_{x_r} are the longitudinal forces, δ means the steering angle and l_r and l_f are the distance from the center of mass of the vehicle to the center of mass of the wheel (r for rear and f for front).

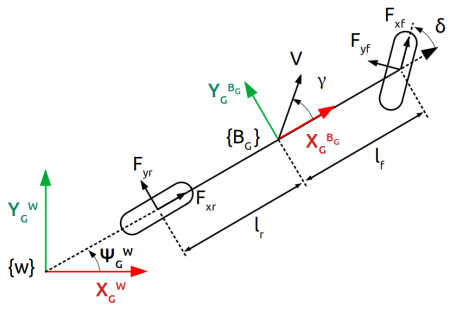

Fig. 5. Forces acting in the vehicle

For simplifying further analysis, it is assumed that there is not slip angle, and the lateral forces F_{y_f} and F_{y_r} are small and can be considered close to zero (the vehicle moves with slow movements). Therefore, the previous model yields

$$\begin{aligned} m\ddot{x}_G^{B_G} &= F_{x_f}(1+\cos(\delta)) + m\dot{y}_G^{B_G}\dot{\psi}_G^{B_G} \\ m\ddot{y}_G^{B_G} &= F_{x_f}\sin(\delta) + m\dot{x}_G^{B_G}\dot{\psi}_G^{B_G} \\ I_z\ddot{\psi}_G^{B_G} &= l_f F_{x_f}\sin(\delta) \end{aligned} \tag{7}$$

considering that $F_{x_r} = F_{x_f}$.

The position and orientation of the ground vehicle can be defined as $q = [\xi_G^{B_G}, \psi_G^{B_G}]^T$ with $\xi_G^{B_G} = [x_G^{B_G}, y_G^{B_G}, z_G^{B_G}]^T$, and $z_G^{B_G} \neq 0$ is considered constant. For further analysis, we use $\xi_{G_{x,y}}^{B_G} = [x_G^{B_G}, y_G^{B_G}]^T$ that corresponds to the position of the ground vehicle in the plane x, y.

Next subsections the controllers for the longitudinal and lateral dynamics are described, they are obtained using ideas from [21].

Longitudinal controller design: Define $e_G^{B_G} = \xi_{G_{x,y}}^{B_G} - \xi_{G_{d_{x,y}}}^{B_G}$ as the error position between the desired position $\xi_{G_{d_{x,y}}}^{B_G}$ and UGV position in the plane x, y. Thus, define a fast terminal sliding surface and its fractional derivative as follows,

$$\begin{aligned} s_1 &= w_{s_1}\dot{e}_{G_x}^{B_G} + w_{s_2}D^{\beta_1-1}(sgn(e_{G_x}^{B_G})|e_{G_x}^{B_G}|^{\alpha_1}) \\ \dot{s}_1 &= w_{s_1}\ddot{e}_{G_x}^{B_G} + w_{s_2}D^{\beta_1}(sgn(e_{G_x}^{B_G})|e_{G_x}^{B_G}|^{\alpha_1}) \end{aligned} \tag{8}$$

where $w_{s_1} > 0$, $w_{s_2} > 0$, $0 < \beta_1 < 1$ and $0 < \alpha_1 < 1$ are constants and $e_{G_x}^{B_G} = [x_G^{B_G} - x_{G_d}^{B_G}]^T$ with $x_{G_d}^{B_G}$ describes the desired position of the ground vehicle in the x axis. Therefore, it follows that $\dot{e}_{G_x}^{B_G} = \dot{x}_G^{B_G} - \dot{x}_{G_d}^{B_G}$. Using the previous, with the first equation in (7) into (8) and considering that the GV moves slowly implies that $\dot{x}_{G_d}^{B_G} << 1$ and can be neglected, then it yields

$$\dot{s}_1 = w_{s_1}\frac{F_{x_f}}{m}(1+cos\delta) + \dot{y}_G^{B_G}\dot{\psi}_G^{B_G} + w_{s_2}D^{\beta_1}(sgn(e_{G_x}^{B_G})|e_{G_x}^{B_G}|^{\alpha_1}) \tag{9}$$

Assuming that the rear and frontal wheels carry half the vehicle mass, it results in half of the total force for each side, therefore without loss of generality, we can propose $F_{x_r} = F_{x_f} = \frac{1}{2}u_1$ where u_1 is the main control input applied to the vehicle.

Then, propose u_1 as,

$$u_1 = \frac{2m}{w_{s_1}(1+cos\delta)}\left(-k_1 sat(s_1) - w_{s_2}D^{\beta_1}(sgn(e_{G_x}^{B_G})|e_{G_x}^{B_G}|^{\alpha_1}) - \dot{y}_G^{B_G}\dot{\psi}_G^{B_G}\right) \tag{10}$$

where $k_1 > 0$ is a constant.

Lateral controller design: Define the error in the lateral position as $e_{G_y}^{B_G} = [y_G^{B_G} - y_{G_d}^{B_G}]^T$ with $y_{G_d}^{B_G}$ describing the desired position of the ground vehicle in the y axis and considered be constant. Then, for controlling the lateral dynamics, we propose

$$e_1 = w_y e_{G_y}^{B_G} + w_\psi f_w \tag{11}$$

where w_y and w_ψ are positive constant parameters, and f_w represents a weighting function containing the heading of the vehicle and is defined as

$$f_w = \frac{e_{G_\psi}^{B_G}}{\rho^{e_2}} \tag{12}$$

with $e_{G_\psi}^{B_G} = \psi_G^{B_G} - \psi_{G_d}^{B_G}$, ρ is a constant parameter value, $e_2 = |e_{G_x}^{B_G}| + |e_{G_y}^{B_G}|$, and $\psi_{G_d}^{B_G}$ defines the desired constant value for the heading. Then from (11), it follows that

$$\begin{aligned} \dot{e}_1 &= w_y\dot{e}_{G_y}^{B_G} + w_\psi\dot{f}_w \\ \ddot{e}_1 &= w_y\ddot{e}_{G_y}^{B_G} + w_\psi\ddot{f}_w \end{aligned} \tag{13}$$

with

$$\begin{aligned} \dot{f}_w &= \frac{\dot{e}_{G_\psi}^{B_G} - e_{G_\psi}^{B_G} ln(\rho)\dot{e}_2}{\rho^{e_2}} \\ \ddot{f}_w &= \frac{\ddot{e}_{G_\psi}^{B_G} - ln(\rho)e_{G_\psi}^{B_G} sgn(e_{G_y}^{B_G})\ddot{e}_{G_y}^{B_G}}{\rho^{e_2}} + c_1 \end{aligned} \tag{14}$$

where,

$$c_1 = \frac{-2ln(\rho)\dot{e}_{G_\psi}^{B_G}\dot{e}_2 + e_{G_\psi}^{B_G} ln(\rho)^2\dot{e}_2^2 - e_{G_\psi}^{B_G} ln(\rho)sgn(e_{G_x}^{B_G})\ddot{x}_G^{B_G}}{\rho^{e_2}} \tag{15}$$

Using (14) for rewriting the second equation of (13), it follows that

$$\ddot{e}_1 = \ddot{e}_{G_y}^{B_G}c_2 + \ddot{e}_{G_\psi}^{B_G}\frac{w_\psi}{\rho^{e_2}} + w_\psi c_1 \tag{16}$$

with

$$c_2 = w_y - \frac{e_{G_\psi}^{B_G} ln(\rho)sgn(e_{G_\psi}^{B_G})w_\psi}{\rho^{e_2}}$$

Propose a fast terminal sliding surface as

$$s_2 = w_{s_3}\dot{e}_1 + w_{s_4}D^{\beta_2-1}(sgn(e_1)|e_1|^{\alpha_2}) \tag{17}$$

where $w_{s_3} > 0$, $w_{s_4} > 0$, $0 < \beta_2 < 1$ and $0 < \alpha_2 < 1$. Then,

$$\dot{s}_2 = w_{s_3}\ddot{e}_1 + w_{s_4}D^{\beta_2}(sgn(e_1)|e_1|^{\alpha_2}) \tag{18}$$

Using (7) and introducing (16) into (18), and assuming that $\ddot{y}_{G_d}^{B_G} << 1$, it yields

$$\begin{aligned} \dot{s}_2 &= w_{s_3}\left(\sin(\delta)F_{x_f}\left(\frac{c_2}{m} + \frac{l_f w_\psi}{I_z\rho^{e_2}}\right) + \dot{x}_G^{B_G}\dot{\psi}_G^{B_G}c_2 + w_\psi c_1\right) \\ &\quad + w_{s_4}D^{\beta_2}(sgn(e_1)|e_1|^{\alpha_2}) \end{aligned} \tag{19}$$

Propose $\sin\delta = u_2$ as our heading control input, and consider that the UGV is moving, implying that $|F_{xf} w_{s_3}| > 0$, therefore u_2 can be proposed as

$$u_2 = \frac{\left(\frac{c_2}{m} + \frac{l_f w_\psi}{I_z \rho^{c_2}}\right)^{-1}}{F_{xf} w_{s_3}} \left(-k_2 sat(s_2) - \dot{x}_G^{B_G} \dot{\psi}_G^{B_G} c_2 - w_\psi c_1 - w_{s_4} D^{\beta_1} (sgn(e_1)|e_1|^{\alpha_1}) \right) \quad (20)$$

2) Stability Analysis: System (7), with the sliding surfaces (8) and (17) and the longitudinal and lateral control laws (10) and (20) is stable in closed loop, i.e., system (7) will achieve the terminal sliding surface with $s = 0$ within a finite time, leading to the convergence of the subsequent error $e_{G_x}^{B_G}$ and e_1 to zero.

Proposing the following Lyapunov candidate

$$V = \frac{1}{2} s_1^2 + \frac{1}{2} s_2^2 \quad (21)$$

then,

$$\dot{V} = s_1 \dot{s}_1 + s_2 \dot{s}_2 \quad (22)$$

Introducing (9), (19), (10) and (20), into the above, it becomes

$$\dot{V} = -s_1 k_1 sat(s_1) - s_2 k_2 sat(s_2) \quad (23)$$

Based on the Lyapunov stability theory, it is evident from the above that the system achieves stability and fulfills the sliding mode arrival conditions when the inequality $\dot{V} \leq 0$ holds true.

V. Results

The experimental setup is depicted in Figure 6, with the white lines denoting the reference path. In this experimental endeavor, a UAV equipped with a downward-facing onboard camera follows a predetermined set of coordinates, $\xi_{A_d}^W$, with $z_{A_d}^W = 2$m of altitude to the ground.

The vision and UGV controller modules were crafted within the ROS framework, while the UAV controller was implemented using Fl-AIR framework. The images transmitted from the UAV's camera exhibit dimensions of 300×300 pixels.

Fig. 6. Experimental setup

1) Control in the image plane: Observe that the goal is to control the UGV in the image plane, therefore, its position $\xi_G^{B_G}$ must be related to the image frame in the following way. Consider that the desired point in the plane x, y for the UGV is given in the body frame of the ground vehicle as $\xi_{G_{d_{x,y}}}^{B_G} = [\ x_{G_d}^{B_G} \quad y_{G_d}^{B_G}\ ]^T$, therefore, its perspective projection in the image plane can be given by

$$\begin{bmatrix} \xi_{G_d}^i \\ 1 \end{bmatrix} z_p^C = \begin{bmatrix} f_x & 0 & 0 \\ 0 & f_y & 0 \\ 0 & 0 & 1 \end{bmatrix} \begin{bmatrix} R_{CB_G} & T_{CB_G} \end{bmatrix} \begin{bmatrix} \xi_{G_{d_{x,y}}}^{B_G} \\ 1 \end{bmatrix} \quad (24)$$

where $\xi_{G_d}^i$ is the projected point on image frame, f_x and f_y represent the camera focal length values retrieved from camera calibration, z_p^C defines the point depth distance in camera coordinate frame, R_{CB_G} and T_{CB_G} are the homogeneous transformation matrix composed by a 3×3 rotation matrix and $3x1$ translation matrix from coordinate frame B_G to C, respectively, see Figure 7.

The UGV is considered to rotate only in the yaw angle ($\psi_G^{B_G}$), therefore, it is assumed that pitch and roll angles are equals to zero. Therefore with out loss of generality, we can consider that $\psi_G^{B_G} = \psi_G^i$. Additionally for practical applications, we assume that the ground can be approximated as a plane, meaning that the plane defined by X^{B_G} and Y^{B_G} is parallel to the plane defined by X^C and Y^C, see Figure 7.

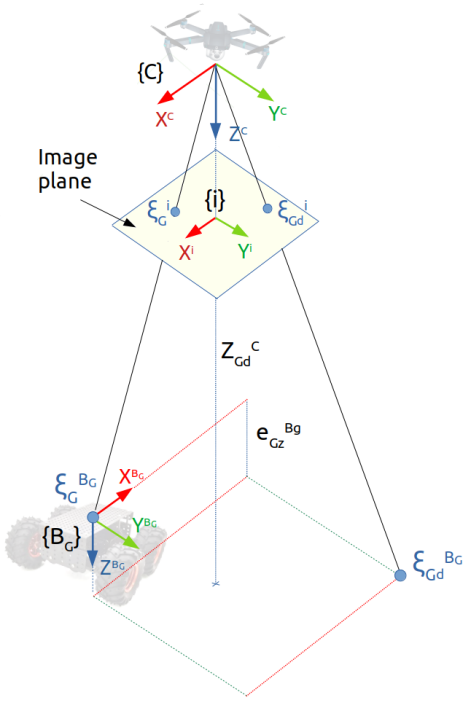

Fig. 7. Perspective projection, three frames are used; the camera frame (C), the image frame (i) and the body frame in the ground vehicle (B_G)

Hence, the error for the UGV between its desired position and the actual position can be formulated as $e_G^{B_G} = \xi_G^{B_G} - \xi_{G_d}^{B_G}$

which can be represented in the image plane as

$$\begin{bmatrix} e^i_G \\ 0 \end{bmatrix} z^C_{G_d} = \begin{bmatrix} f_x & 0 & 0 \\ 0 & f_y & 0 \\ 0 & 0 & 1 \end{bmatrix} R_{CB_G} e^{B_G}_G - \begin{bmatrix} \xi^i_G \\ 1 \end{bmatrix} e^{B_G}_{G_z} \quad (25)$$

where $e^i_G = [\ e^i_{G_x} \quad e^i_{G_y}\ ]^T$ is the error in image frame. Notice that the ArUco marker is placed atop the UGV, therefore $z^{BG}_G \neq 0$, then there is a difference in depth between the ground and the marker, this difference is denoted by $e^{B_G}_{G_z}$, and its value is equal to the UGV height. The depth distance of the ground in camera frame is expressed as $z^C_{G_d}$.

Rearranging equation (25) and defining $r_{B_GC_1}$ and $r_{B_GC_2}$ as the first and second row of matrix $R^{-1}_{CB_G}$, we find that,

$$\begin{aligned} e^{B_G}_{G_x} &= r_{B_GC_1} M^{-1} \begin{bmatrix} e^i_G z^C_{G_d} + \xi^i_G e^{B_G}_{G_z} \\ e^{B_G}_{G_z} \end{bmatrix} \\ &= r_{B_GC_1} M^{-1} A^i \\ e^{B_G}_{G_y} &= r_{B_GC_2} M^{-1} \begin{bmatrix} e^i_G z^C_{G_d} + \xi^i_G e^{B_G}_{G_z} \\ e^{B_G}_{G_z} \end{bmatrix} \\ &= r_{B_GC_2} M^{-1} A^i \end{aligned} \quad (26)$$

Then,

$$\begin{aligned} \dot{e}^{B_G}_{G_x} &= s_{k_1} R_{B_GC} M^{-1} A^i + r_{B_GC_1} M^{-1} \dot{A}^i \\ \dot{e}^{B_G}_{G_y} &= s_{k_2} R_{B_GC} M^{-1} A^i + r_{B_GC_2} M^{-1} \dot{A}^i \end{aligned} \quad (27)$$

with s_{k_1} and s_{k_2} are first and second row of the Skew-symmetric matrix S_k, where

$$S_k = \begin{bmatrix} 0 & -\dot{\psi}^i_G & 0 \\ \dot{\psi}^i_G & 0 & 0 \\ 0 & 0 & 0 \end{bmatrix}$$

and

$$\dot{A}^i = \begin{bmatrix} \dot{e}^i_G z^C_{G_d} + \dot{\xi}^i_G e^{B_G}_{G_z} \\ 0 \end{bmatrix}$$

Therefore, with the above procedure it is easy to compute the control inputs in the image plane for being applied in experiments.

2) Experimental tests:

As explained before, the experiment consists that the aerial vehicle must follow a trajectory previously defined, where its coordinates in $x-y$ plane closely aligns (for better illustrate the results) with the center-line path formed by two white lines, see figure 6. The goal of this experiment is to autonomous navigate the UGV in the middle of these 2 white lines (orange line in the figure) using only information coming from the aerial vehicle. Notice that the UGV does not know the road and its position. It is located in the image plane of the aerial vehicle that gives the trajectory to follow.

The experimental results are depicted in the figures bellow. In Figure 8 the trajectories performances obtained by the UGV and UAV are illustrated. Notice in this figures the well performance of the ground vehicle, and the close similarity of the performed trajectory with the path shown in Figure 6. Figures 9 - 11 display the deviations observed (errors) in the image frame while Figures 13 and 12 the control signals applied to the ground vehicle and the its velocity are illustrated.

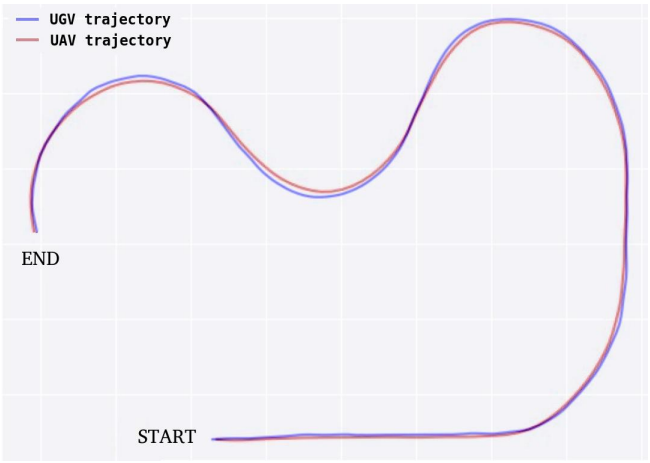

Fig. 8. UGV and UAV trajectories performances.

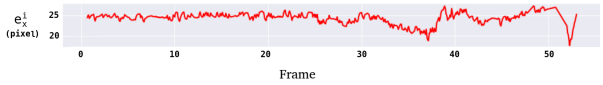

Fig. 9. UGV longitudinal error in the image frame during its autonomous navigation.

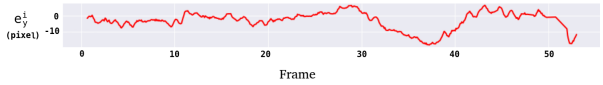

Fig. 10. UGV lateral error obtained in the image frame during tests.

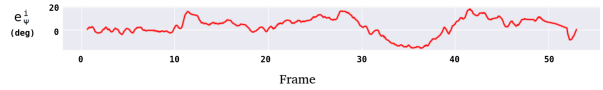

Fig. 11. Resulted yaw error during navigation

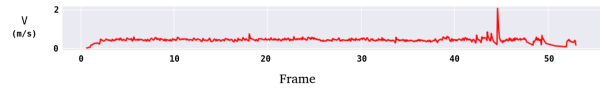

Fig. 12. Resulted velocity during navigation

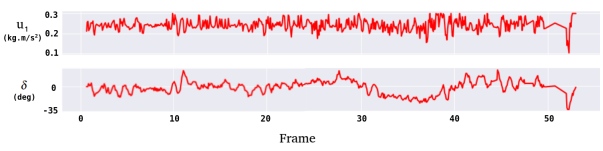

Fig. 13. Resulted controller outputs during navigation

It is worth mentioning that the UAV was configured to operate at a relatively low velocity, ensuring that the UGV could effectively keep pace with the UAV throughout the navigation process. This deliberate choice aimed to prevent the UAV from advancing too far and losing sight of the UGV within its camera field of view.

From graphs and video, it was demonstrated that our system has proven its ability to effectively guide the Unmanned Ground Vehicle (UGV) in close adherence to the predefined reference path. This achievement serves as a robust validation of the efficacy of our control laws in maintaining the UGV in the desired path. Furthermore, it is pertinent to highlight the deliberate and consistent low-velocity profile exhibited by the UGV, which is consistent with our intended operational strategy. Remark that this work does not consider high velocity.

Observe also from Figure 9 that the positional error in the x-coordinate consistently remained around 25 pixels. In accordance with prior explanations, the vision module strategically positions the desired point ahead of the UGV, with a fixed distance along the path. This outcome aligns with our expectations since the UGV persistently pursued a predefined point ahead on the path, introducing this minor deviation. Similarly, errors in the y-coordinate and angular error primarily hovered around zero, with higher variations occurring during the vehicle's traversal through curved segments of the path.

A video of this experiment can be see at : https://youtu.be/MNFaOl3y6GI.

VI. Conclusion and future work

In conclusion, the outcomes of this study demonstrated the successful cooperation between Unmanned Ground Vehicles and Unmanned Aerial Vehicles through the implementation of the proposed Aerial Vision-Based Guidance and Control System. The system effectively guided a ground vehicle devoid of perception sensors along a predefined path for the aerial vehicle, highlighting its potential in various applications.

The efficacy of both modules (vision and controller) were well proved, showing that it is possible to guide a ground vehicle using only aerial information. From a control point of view, the new control algorithm for the ground vehicle performed well and its stability was proved using the Lyapunov theory.

These findings suggest a promising foundation for further research and development. Future work should concentrate on designing a UAV controller that can guarantee the sustained presence of both the path and the UGV within its camera field of view during navigation. This will be especially critical in scenarios where the ground vehicle may need to deviate from the path temporarily, such as when avoiding critical regions. Ensuring continuous aerial visibility of the UGV is imperative to prevent the loss of control and maintain effective coordination between the UAV and UGV.

References

[1] T. Miki, P. Khrapchenkov, and K. Hori, "Uav/ugv autonomous cooperation: Uav assists ugv to climb a cliff by attaching a tether," *2019 International Conference on Robotics and Automation (ICRA)*, pp. 8041–8047, 2019.

[2] S. Kiribayashi, J. Ashizawa, and K. Nagatani, "Modeling and design of tether powered multicopter," *2015 IEEE International Symposium on Safety, Security, and Rescue Robotics (SSRR)*, pp. 1–7, 2015.

[3] D. H. Nguyen, "A nature-inspired distributed robust control design for ground-aerial vehicle cooperation," *IEEE Transactions on Intelligent Transportation Systems*, vol. 24, pp. 4454–4463, 2023.

[4] L. Cantelli, M. Mangiameli, C. D. Melita, and G. Muscato, "Uav/ugv cooperation for surveying operations in humanitarian demining," *2013 IEEE International Symposium on Safety, Security, and Rescue Robotics (SSRR)*, pp. 1–6, 2013.

[5] C. Potena, R. Khanna, J. I. Nieto, R. Y. Siegwart, D. Nardi, and A. Pretto, "Agricolmap: Aerial-ground collaborative 3d mapping for precision farming," *IEEE Robotics and Automation Letters*, vol. 4, pp. 1085–1092, 2018.

[6] A. Gawel, Y. Lin, T. Koutros, R. Y. Siegwart, and C. Cadena, "Aerial-ground collaborative sensing: Third-person view for teleoperation," *2018 IEEE International Symposium on Safety, Security, and Rescue Robotics (SSRR)*, pp. 1–7, 2018.

[7] J. qiang Li, G. Deng, C. Luo, Q. Lin, Q. Yan, and Z. Ming, "A hybrid path planning method in unmanned air/ground vehicle (uav/ugv) cooperative systems," *IEEE Transactions on Vehicular Technology*, vol. 65, pp. 9585–9596, 2016.

[8] H. Kandath, T. Bera, R. Bardhan, and S. Sundaram, "Autonomous navigation and sensorless obstacle avoidance for ugv with environment information from uav," *2018 Second IEEE International Conference on Robotic Computing (IRC)*, pp. 266–269, 2018.

[9] J. H. Kim, J.-W. Kwon, and J. Seo, "Multi-uav-based stereo vision system without gps for ground obstacle mapping to assist path planning of ugv," *Electronics Letters*, vol. 50, pp. 1431–1432, 2014.

[10] B. R. Chang, H. F. Tsai, and J.-L. Lyu, "Drone-aided path planning for unmanned ground vehicle rapid traversing obstacle area," *Electronics*, 2022.

[11] S. S. Mehta, W. E. Dixon, D. M. Arthur, and C. D. Crane, "Visual servo control of an unmanned ground vehicle via a moving airborne monocular camera," *2006 American Control Conference*, pp. 6 pp.–, 2006.

[12] X. Liang, H. Wang, Y. Liu, B. You, Z. Liu, and W. Chen, "Calibration-free image-based trajectory tracking control of mobile robots with an overhead camera," *IEEE Transactions on Automation Science and Engineering*, vol. 17, pp. 933–946, 2020.

[13] C. Chen, Y. Wan, B. Li, C. Wang, G. Xie, and H. Jiang, "Motion planning for heterogeneous unmanned systems under partial observation from uav," *2020 IEEE/RSJ International Conference on Intelligent Robots and Systems (IROS)*, pp. 1474–1479, 2020.

[14] M. F. Santos and A. C. Victorino, "Autonomous vehicle navigation based in a hybrid methodology: model based and machine learning based," *2021 IEEE International Conference on Mechatronics (ICM)*, pp. 1–6, 2021.

[15] D. A. de Lima and A. C. Victorino, "A visual servoing approach for road lane following with obstacle avoidance," *17th International IEEE Conference on Intelligent Transportation Systems (ITSC)*, pp. 412–417, 2014.

[16] K. S. Miller and B. Ross, "An introduction to the fractional calculus and fractional differential equations," 1993.

[17] S. Pooseh, R. Almeida, and D. F. M. Torres, "Numerical approximations of fractional derivatives with applications," *Asian Journal of Control*, vol. 15, no. 3, pp. 698–712, 2013.

[18] S. Pooseh, R. Almeida, and D. F. M. Torres, "Approximation of fractional integrals by means of derivatives," *Comput. Math. Appl.*, vol. 64, pp. 3090–3100, 2012.

[19] J. Carino, H. Abaunza, and P. Castillo, "A fully-actuated quadcopter representation using quaternions," *International Journal of Control*, 2022.

[20] D. Müllner, "Modern hierarchical, agglomerative clustering algorithms," *ArXiv*, vol. abs/1109.2378, 2011.

[21] Y. Feng, X. Yu, and F. Han, "On nonsingular terminal sliding-mode control of nonlinear systems," *Autom.*, vol. 49, pp. 1715–1722, 2013.